Development of Intrinsically Photoluminescent and Photostable Polylactones

*Zhiwei Xie, Yi Zhang, Li Liu, Hong Weng, Ralph P. Mason, Liping Tang, Kytai T. Nguyen, Jer-Tsong Hsieh, and Jian Yang**

The use of biodegradable polymers, in particular hydrolytically degradable polylactones such as polylactide (PLA), polyglycolide (PGA), and their copolymers (PLGA), has generated a huge scientific and economic impact on a broad range of biomedical applications such as disposable medical devices, tissue engineering, drug delivery, and molecular targeting.[1,2] However there have only been few innovations in new design of polylactone materials to meet the ever-growing need for functional biomaterials in medical applications, especially where new bioimaging techniques including optical imaging have become important enabling tools for innovation.[3] Herein, we report a series of newly developed biodegradable polylactone copolymers possessing photostable and in vivo detectable intrinsic fluorescence without conjugating or encapsulating traditional photobleaching organic dyes or cytotoxic semiconducting quantum dots. We also demonstrate the applications of these new materials for in vivo real-time tracking of scaffold degradation and for theranostic cancer treatment.

Despite the exciting progress, some fundamental understandings on the key elements of tissue engineering are still lacking. For example, although it has been recognized that the scaffold degradation rate should match the rate of new tissue formation, biomaterial designs to control the in vivo scaffold degradation rate remain empirical due to the lack of quantitative in vivo validation. Currently, in vivo scaffold degradation is often estimated based on the outcomes of in vitro degradation measurements.[4,5] Unfortunately, various factors have been shown to affect biomaterial degradation in vivo, which cannot be precisely simulated in vitro.[6] Attempts to quantify polymeric scaffold degradation in vivo have been inconsistent due to the difficulty of separating the infiltrated/regenerated tissues from the porous scaffolds.[6] An in situ real-time method to accurately monitor and quantify scaffold degradation and tissue regeneration processes without traumatically explanting samples or sacrificing animals is urgently needed.[2,7] To achieve this goal, it is essential that the biodegradable polymers can be used as non-invasive bioimaging probes, in addition to providing a suitable cell growth substrate. Recently, fluorescent dye conjugated polyethylene glycol (PEG)/dextran hydrogels were developed to track the in vivo material degradation.[7] However, such a model system may bring about concerns of photobleaching and cytotoxicity that are often associated with the use of traditional organic dyes. The loss of the conjugated fluorescent dyes on the polymers may complicate the understanding on fluorescence loss and material degradation.

Biodegradable polymers, mostly polylactones, have also been widely used as theranostic nanomedicine platforms for targeted drug delivery and high-throughput imaging.[8] Generally, imaging agents alone cannot be used as drug delivery carriers and vice versa. Therefore, the conjugation/encapsulation of imaging agents onto/into drug delivery carriers is normally required to generate theranostic nanobiomaterials. Polymeric nanoparticles are usually conjugated with additional organic dyes or quantum dots (QDs) for fluorescence imaging.[9] However, the poor photobleaching-resistance and low dye-to-particle conjugation ratios of organic dyes as well as the toxicity and poor hydrodynamic stability of QDs prevent their practical uses in vivo.[10] Encapsulating/conjugating imaging agents in/on nanoparticles may result in increased particle sizes, added complexity, and higher risk of adverse biological reactions.[11] Moreover, targeting ligands have to share conjugation sites with imaging agents, which may result in insufficient conjugation, thus reducing both the targeting and imaging efficiency.[12] Such challenges might be resolved by using biodegradable fluorescent polymers that exhibit dual-functionality as drug delivery carriers and imaging probes.

To address the aforementioned concerns, we create a method to develop biodegradable imaging-detectable polymers, biodegradable photoluminescent polylactones (BPLPLs), via a ring-opening polymerization of lactones initiated by our recently developed biodegradable photoluminescent polymers (BPLPs).[13,14] BPLPs are fully degradable pre-polymers that are synthesized by a polycondensation reaction of biocompatible monomers such as citric acid, α-amino acids, and diols.[13] BPLPs display high quantum yields (up to 79%),

Z. Xie, Prof. J. Yang
Department of Biomedical Engineering
Materials Research Institute
The Huck Institutes of The Life Sciences
The Pennsylvania State University
University Park
PA 16802, USA
E-mail: jxy30@psu.edu
Y. Zhang, H. Weng, Prof. L. Tang, Prof. K. T. Nguyen
Department of Bioengineering
The University of Texas at Arlington
Arlington, TX 76019, USA
L. Liu, Prof. R. P. Mason
Department of Radiology
The University of Texas Southwestern Medical Center
Dallas, TX 75390, USA
Prof. J.-T. Hsieh
Department of Urology
The University of Texas Southwestern Medical Center
Dallas, TX 75390, USA

DOI: 10.1002/adma.201306070

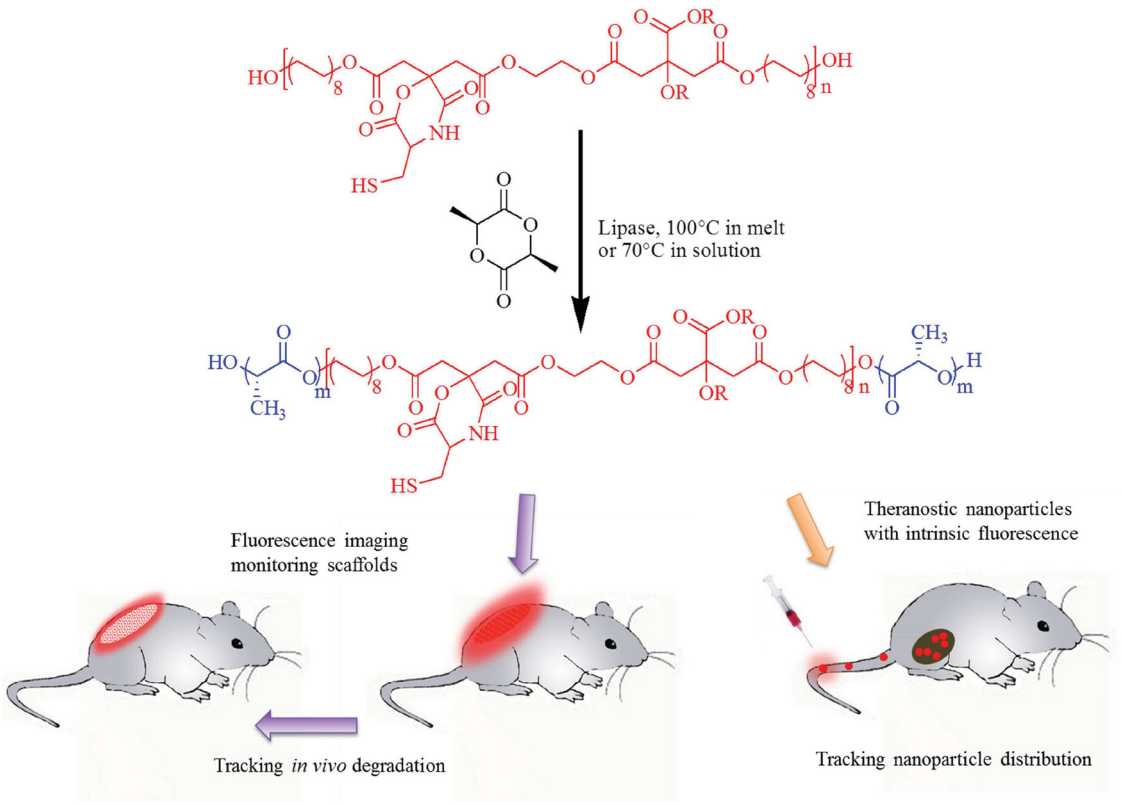

Figure 1. Schematic illustration of biodegradable photoluminescent polylactide (BPLPL-Cys-PLLA) synthesis and its applications in scaffold imaging and nanoparticle tracking in vivo.

tunable fluorescence emission with varied amino acids (up to 725 nm), and superior photostability compared to organic dyes.[13–15] Herein, for the first time, we report the synthesis and characterization of thermoplastic BPLPLs, exemplified by BPLP-*co*-Poly(L-lactide) (BPLP-PLLA). The hydroxyl or carboxyl groups of BPLPs initiate ring-opening polymerization of lactone monomers such as lactide, glycolide, and caprolacone to make completely degradable block copolymers (BPLPLs) (**Figure 1**a). The resulting BPLPL copolymers retained the intrinsic photoluminescence inherited from BPLPs, which enabled the feasibility of non-invasive imaging for monitoring the BPLPL scaffold degradation and tracking of cancer targeting BPLPL nanoparticles in vivo (Figure 1b and 1c).

The synthesis route of BPLP-PLLA copolymer is illustrated in Figure 1a. The BPLP:lactide molar ratios were varied as 1:20, 1:50, and 1:100. For example, BPLP-Cys-PLLA20 represents a copolymer that was synthesized from BPLP with L-cysteine as the amino acid component and the feeding molar ratio of BPLP-Cys to L-lactide of 1:20. As presented in our previous work,[13] water-soluble BPLPs (WBPLPs) were made with hydrophilic polyethylene glycol (PEG) chosen as the diol. Therefore, amphiphilic biodegradable photoluminescent WBPLP-PLLAs were also synthesized with WBPLP as the hydrophilic block and PLLA as the hydrophobic block. All polymers synthesized are summarized in Supplementary Table S1. ^{1}H NMR and FTIR confirm that the chemical structures of BPLP-PLLAs (Figure S1 and S2, Supporting Information) consist of functional groups from both BPLPs and PLLA.

All BPLP-PLLA copolymers emitted strong fluorescence, as shown in **Figure 2**a and 2b. For BPLP-Cys-PLLA, the maximum emission (441 nm) and excitation (377 nm) had slightly different from that of BPLP-Cys pre-polymer, which had maximum emission and excitation wavelengths of 434 and 365 nm, respectively.[13,14] At the same concentration (10 mg/mL), the longer PLLA blocks were, the relatively weaker fluorescent intensity was observed. BPLP-Ser-PLLA also emits tunable fluorescent light depending on the excitation wavelength as similar to BPLP-Ser.[13,14] As shown in Figure 2b, BPLP-Ser-PLLA50 displayed fluorescence emissions from 350 nm to 700 nm. In addition, BPLP-Cys-PLLA copolymers provided exceptionally high quantum yields (up to 51.4%, Table S1, Supporting Information), which are in the range of traditional fluorescent materials, including organic dyes, quantum dots, and green fluorescent proteins.[15] One exceptional advantage of the BPLPs is the excellent photostability over traditional organic dyes. BPLP-PLLAs inherit this property, which is a key feature for many bioimaging applications,[16] from BPLPs by showing much better photo-bleaching resistance against continuous illumination over photobleaching organic dyes, e.g. Rhodamine B and Fluorescein. (Figure 2c). The BPLP-PLLA polymers all possessed outstanding photostability with >90% signal remaining even after a long (3 hours) illumination. These intriguing fluorescence properties will empower our novel degradable BPLPLs for both in vitro and in vivo detections.

The thermal properties of BPLP-PLLAs were characterized by Differential Scanning Calorimetry (DSC) and Thermal

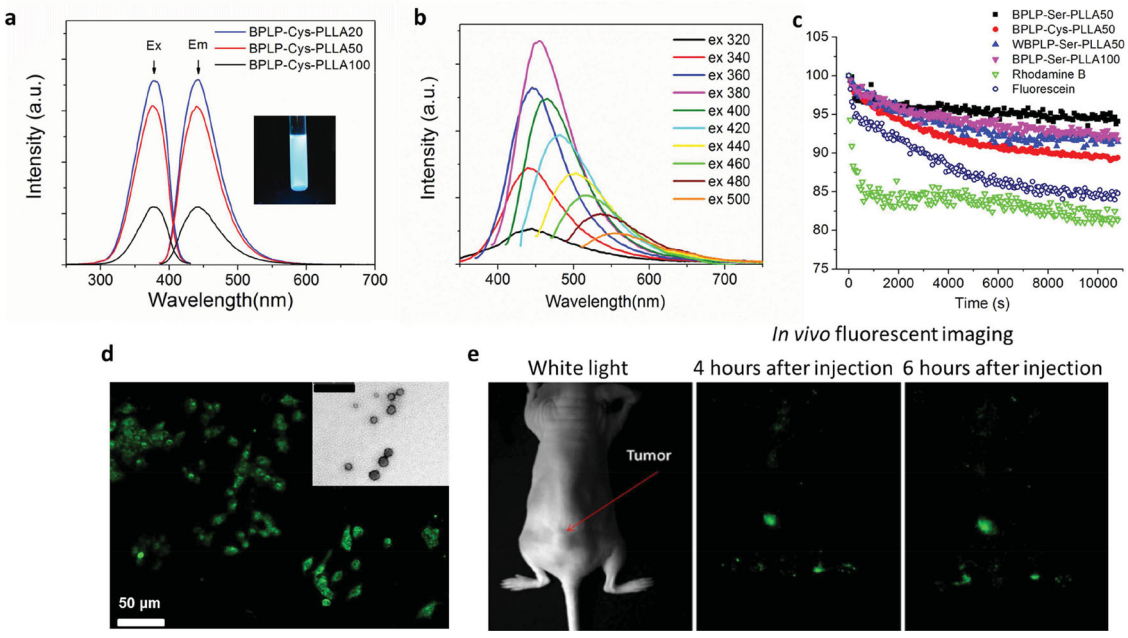

Figure 2. Photoluminescent and imaging characterizations of BPLP-PLLAs. a) Fluorescent excitation and emission spectra of BPLP-Cys-PLLA with various polylactide chain lengths (insert, optical imaging of BPLP-Cys-PLLA50 solution under UV light). b) Fluorescent emission spectra of BPLP-Ser-PLLA50 shift depending on the excitation wavelengths (320 nm to 500 nm). c) Photostability of various BPLP-PLAs polymer solutions compares to Rhodamine B and Fluorescein solutions that were subjected to 3 hours of continuous illumination. d) Fluorescence microscopic image of 3T3 mouse fibroblasts with BPLP-Ser-PLLA50 nanoparticles uptaken (insert, TEM image of BPLP-Ser-PLLA50 nanoparticles, insert scale bar = 100 nm). e) Representative in vivo white light and fluorescence images of a nude mouse with a human MCF7 breast tumor xenograft growing on its back after tail intravenous injection of BPLP-Ser-PLLA50 nanoparticles.

Gravimetric Analysis (TGA). Figure S3a (Supporting Information) presents the DSC thermograms of BPLP-Cys-PLLA copolymers with various PLLA chain lengths. The glass transition temperature (Tg) increases gradually with the increasing of PLLA block lengths: 0, 12.2, and 40.1 °C for BPLP-Cys-PLLA20, BPLP-Cys-PLLA50, and BPLP-Cys-PLLA100, respectively. The same trend could also apply to BPLP-Ser-PLLA and WBPLP-PLLA (Figure S4, Supporting Information). Figure S3b (Supporting Information) also shows a representative DSC thermogram of BPLP-Cys-PLLA100 with a clear crystallization peak at 106.1 °C and a melting peak at 115.3 °C, which is lower than the typical melting point of PLLA (around 170 °C),[17] probably due to the incorporation of softer BPLP chains. Figure S5 (Supporting Information) characterizes the thermal decomposition temperatures of BPLP-Cys-PLLA copolymers. BPLP-Cys-PLLA20 exhibited a slight weight loss at 120 °C, possibly due to the loss of water from carboxyl group. However, no weight loss was observed before 280 °C for BPLP-Cys-PLLA100, in common with commercial PLLA.[17] Unlike BPLPs, all BPLPLs could not be thermally crosslinked upon heating, suggesting they are thermoplastic materials. With similar thermal properties to PLLA, our BPLP-PLLAs can be processed into various forms, including films, scaffolds, particles, micelles and fibers for a broad range of biomedical applications. BPLP-Ser-PLLA particle sizes and drug delivery profiles can also be easily tuned by varying the molecular design of polymers (Figure S6, Supporting Information). Previously mentioned amphiphilic WBPLP-PLLAs were also prepared into micelles with controllable critical micelle concentration (Figure S7, Supporting Information). Both nanoparticles and micelles exhibited strong fluorescence in aqueous solutions (Figure S8, Supporting Information). Importantly, BPLP-Ser-PLLA50 nanoparticles that were taken up by 3T3 fibroblasts in vitro could be imaged by fluorescent microscopy, verifying the cell labeling capability of BPLPLs that is similar to fluorescent dyes and quantum dots (Figure 2d). BPLP-PLLA nanoparticles were also tested as drug delivery carriers using 5- fluorouracil as a model drug and the release profile was tailored simply by varying the molecular weight of PLLA chain (Figure S9, Supporting Information). In addition, BPLP-Ser-PLLA50 polymers were electrospun into uniform ultra-fine fibers that exhibited strong photoluminescence (Figure S10, Supporting Information). Electrospun fibers have been widely used in tissue engineering as the nano-fibrous structures mimic the structures of extracellular matrix such as collagen and elastin. Thus, BPLPLs demonstrate excellent processability, which is exemplified by the fabrication of films, particles, fibers and scaffolds suggesting that BPLPLs may serve as candidate materials for a number of biomedical applications such as tissue engineering, drug delivery, and bioimaging.

To assess the cytotoxicity of BPLPLs, BPLP-Cys-PLLA nanoparticles were cultured with mouse 3T3 fibroblasts. As shown in Figure S11 (Supporting Information) BPLP-Cys-PLLA nanoparticles exhibit lower cytotoxicity than the pristine BPLP-Cys nanoparticles at high concentrations and similar toxicity in vitro to the widely used PLLA nanoparticles. To assess the in vivo host response of BPLP-PLLA, BPLP-Ser-PLLA20 films were implanted subcutaneously in 1-year-old male Sprague Dawley rats. PLLA (Mw = 20 kDa) films and crosslinked BPLP-Ser films

were chosen as controls. Histological analysis showed the presence of inflammatory cells at both 1 and 10 weeks of implantation (Figure S12, Supporting Information). After 1 week of implantation, the acute inflammatory response was mild for all samples. There was no significant difference ($p > 0.05$) observed among PLLA, CBPLP films and BPLP-Ser-PLLA20 in terms of cell density surrounding the implants, while the cell numbers for all samples decreased significantly ($p \ll 0.01$) at week 10 (Figure S12b). Noticeably, the fibrotic capsule thicknesses for CBPLP and BPLP-Ser-PLLA20 was significantly thinner than that for PLLA ($p \ll 0.01$) at both week 1 and week 10 (Figure S12c), likely due to the soft, elastic and hydrophilic nature of CBPLP and BPLP-Ser-PLLA20 compared to PLLA. The fibrotic capsule layer thickness for each sample also decreased and stabilized at week 10. One week after the implantation, CD11b+ inflammatory cell were identified around the implanted materials (Figure S12a). This immunohistochemical analysis (Figure S12d) revealed almost the same number of CD11b+ inflammatory cells around CBPLP and BPLP-Ser-PLLA20 implants as around PLLA (p 0.05). The above animal studies indicated that BPLP-PLLAs generated comparable or even better in vivo tissue responses as compared to the commercial PLLA.

Degradation is a critical property of biomaterials, since it affects cytotoxicity, cell penetration/proliferation, drug release rate, mechanical performance, and many other properties.[18] As expected, the in vitro weight loss of BPLP-PLLAs mainly depended on the length of hydrophobic PLLA blocks (**Figure 3**a). BPLP-Cys-PLLA20 completely degraded after 12 weeks of incubation in PBS, while the degradation rate of BPLP-Cys-PLLA100 was similar to that of PLLA homopolymer with a similar molecular weight.[19] One of the most significant advantages of BPLP-PLLAs is that their degradation can be measured by fluorescent signal decay in addition to the traditional weight loss measurements. We first confirmed that the normalized fluorescence signal loss matched the weight loss of BPLP-PLLAs in vitro (correlation coefficient of two covariance = 0.997) (Figure 3b). This phenomenon supports our hypothesis that fluorescence decay can be used as a measurement of material degradation. Thus, we can monitor the in vivo degradation of BPLP-PLLAs non-invasively by tracking the fluorescence decay of polymers under an in vivo fluorescent imaging system without extracting the implants or sacrificing animals (Figure 3d). As shown in Figure 3c, the weight of BPLP-Ser-PLLA20 decreased much faster in PBS in vitro than in the living body at all time points, especially for the first 5 weeks (correlation coefficient = 0.946), likely due to the relatively large volume of liquid in in vitro degradation compared to the relatively small volume of subcutaneous fluid in animals. Interestingly, by comparing in vivo fluorescence decay and in vivo material degradation, we found that the rate of fluorescence loss was slightly higher than the rate of actual weight loss in first two weeks, and observed a significantly higher fluorescence signal loss at week 3. Although the cause has yet to be determined, it is possible that the acute inflammatory cells and protein-rich interstitial fluids block some fluorescence.[20] Nonetheless, the fluorescence decay still showed a better correlation to the in vivo weight loss compared to in vitro weight loss. When acute inflammation (loose connective tissues) is transformed into mild chronic inflammation (thin fibrotic capsules) after 4 weeks, it is expected that fluorescence decay should better represent the actual material degradation.[5,21] Indeed, we observe that the fluorescence decay after 4 weeks matched (correlation coefficient = 0.987) the in vivo weight loss of the BPLP-Ser-PLLA20 samples. Histological images also confirm that after 10 weeks in vivo implantation, BPLP-Ser-PLLA20 films degraded into small pieces and the infiltrated tissues occupied the spaces of the degraded materials (Figure S13, Supporting Information). Overall, these results indicated that our BPLP-PLLAs provide intrinsic fluorescence, which enabled accurate, non-invasive monitoring of the implant degradation

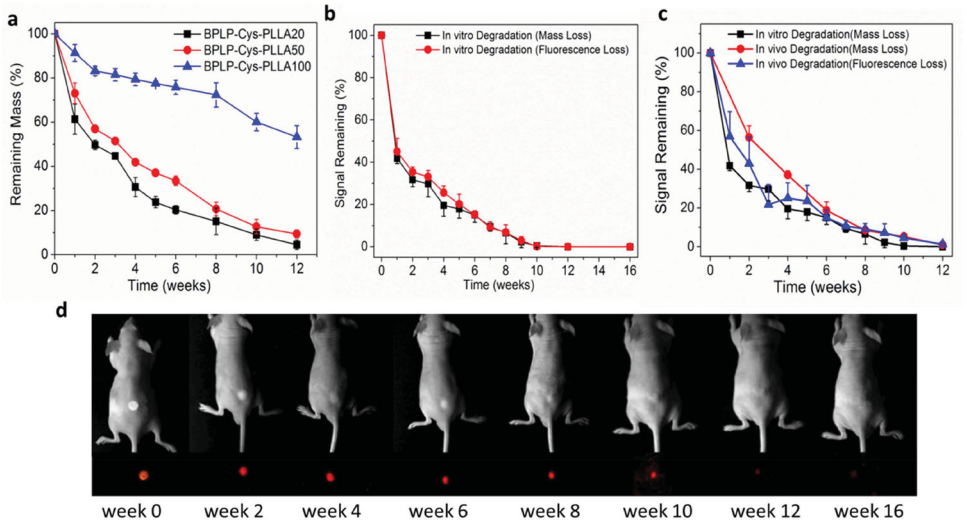

Figure 3. Degradation profiles of BPLP-PLLAs. a) In vitro weight loss in PBS of BPLP-Cys-PLLA with different polylactide chain lengths at 37 °C. b) Comparison of in vitro fluorescence loss and in vitro weight loss of BPLP-Ser-PLLA20. c) Comparison of in vivo fluorescence loss, in vitro weight loss, and in vivo weight loss of BPLP-Ser-PLLA20. d) Top, white light images of a representative nude mice with a subcutaneously implanted BPLP-Ser-PLLA20 film at different time points; bottom, in vivo fluorescent images of the same implant at each time point.

in vivo. It is noteworthy that BPLPs and PLA are all aliphatic polyesters, thus the degradation mechanism of both is the hydrolysis of ester bonds. During a bulk degradation process, the ester bonds cleaved randomly, resulting in that fluorescence loss rate matches the whole polymer degradation rate. Conferring in vivo detectable fluorescent properties to biodegradable polymers may advance the field of tissue engineering as the enabling imaging tool may facilitate obtaining the true understanding on material degradation and tissue material interactions in situ and in real time.

With the unique intrinsic fluorescence, BPLP-PLLAs can be used as a label-free in vivo imaging tool for cancer detection and treatment. To demonstrate the feasibility, targeting ligand folates were conjugated on BPLP-Ser-PLLA50 nanoparticles,[22] which were stable in physiological conditions (Figure S14, Supporting Information). After i.v. injection through the tail vein, these nanoparticles quickly accumulated at the dorsal orthotopic breast tumors (MCF7 cell injected subcutaneously) of a nude mouse within 4–6 hours as detected by in vivo fluorescent imaging system (Figure 2e). Ex vivo fluorescent imaging (Figure S15, Supporting Information) confirms that substantial higher fluorescent intensities were found in tumor tissue than in liver. These results support that BPLP-PLLAs nanoparticle preferentially accumulated at tumor sites. Since drugs can also be easily encapsulated with BPLP-PLLA nanoparticles as well (Figure S9), the feasibility of applying BPLPLs into theranostic cancer management is obvious. Furthermore, the high targeting efficiency is probably a result of high density of targeting folates on the nanoparticle surfaces, since folates do not need to share conjugation sites with imaging molecules as in most existing nanoparticle systems.[23] Thus, our BPLP-PLLA nanoparticles can potentially serve as ideal candidates for in vivo cancer fluorescence imaging and drug delivery, without the need of conjugation with any organic dyes or quantum dots.

In conclusion, we have successfully synthesized and characterized biodegradable photoluminescent polylactone (BPLPL), representatively BPLP-PLLA copolymers. These fully degradable polymers exhibited similar thermal properties and biocompatibility to the commercial polylactones. Most importantly, BPLPLs enabled non-invasive fluorescence imaging for tracking in vivo degradation of polymers. BPLPLs can be fabricated into different forms such as nanoparticles for potential theranostic applications. We demonstrated that incorporating BPLP units into biodegradable polymer design can be an effective way to integrate intrinsically photoluminescent properties into biodegradable polymers. Given the already significant impact generated by using polylactone materials, conferring intriguing in vivo detectable photobleaching-resistant photoluminescence to polylactone represents an innovation that should advance the understanding, design, and use of biodegradable polymers in a broad range of biomedical and biological applications where fluorescence imaging and sensing have gained increasing importance.

Experimental Section

Experimental details are described in the Supporting Information.

Supporting Information

Supporting Information is available online from the Wiley Online Library or from the author. A detailed experimental section is provided.

Acknowledgements

This work was supported in part by a National Institutes of Health Awards (NIBIB EB012575, NCI CA182670, NHLBI HL118498), and National Science Foundation (NSF) Awards (DMR1313553, CMMI 1266116).

Received: December 11, 2013
Revised: March 1, 2014
Published online: March 26, 2014

[1] a) L. L. Hench, J. M. Polak, *Science* **2002**, *295*, 1014; b) R. Langer, D. A. Tirrell, *Nature* **2004**, *428*, 487; c) M. P. Lutolf, J. A. Hubbell, *Nat. Biotech.* **2005**, *23*, 47; d) Y. Wang, G. A. Ameer, B. J. Sheppard, R. Langer, *Nat. Biotech.* **2002**, *20*, 602; e) L. S. Nair, C. T. Laurencin, *Prog. Polym. Sci.* **2007**, *32*, 762; f) H. Tian, Z. Tang, X. Zhuang, X. Chen, X. Jing, *Prog. Polym. Sci.* **2012**, *37*, 237.
[2] M. Vert, *Biomacromolecules* **2005**, *6*, 538.
[3] V. Ntziachristos, *Annu. Rev. Biomed. Eng.* **2006**, *8*, 1.
[4] a) J. Yang, A. R. Webb, G. A. Ameer, *Adv. Mater.* **2004**, *16*, 511; b) Y. Gong, Q. Zhou, C. Gao, J. Shen, *Acta Biomater.* **2007**, *3*, 531.
[5] J. Dey, H. Xu, J. Shen, P. Thevenot, S. R. Gondi, K. T. Nguyen, B. S. Sumerlin, L. Tang, J. Yang, *Biomaterials* **2008**, *29*, 4637.
[6] L. Lu, S. J. Peter, M. D. Lyman, H.-L. Lai, S. M. Leite, J. A. Tamada, S. Uyama, J. P. Vacanti, L. Robert, A. G. Mikos, *Biomaterials* **2000**, *21*, 1837.
[7] N. Artzi, N. Oliva, C. Puron, S. Shitreet, S. Artzi, A. bon Ramos, A. Groothuis, G. Sahagian, E. R. Edelman, *Nat. Mater.* **2011**.
[8] a) J. V. Jokerst, S. S. Gambhir, *Acc. Chem. Res.* **2011**, *44*, 1050; b) A. S. Wadajkar, T. Kadapure, Y. Zhang, W. Cui, K. T. Nguyen, J. Yang, *Adv. Healthc. Mater.* **2012**, *1*, 450.
[9] a) X. Gao, Y. Cui, R. M. Levenson, L. W. K. Chung, S. Nie, *Nat. Biotech.* **2004**, *22*, 969; b) J. V. Jokerst, S. S. Gambhir, *Accounts of Chemical Research* **2011**, *44*, 1050.
[10] a) A. M. Smith, H. Duan, A. M. Mohs, S. Nie, *Advanced Drug Delivery Reviews* **2008**, *60*, 1226; b) H. Soo Choi, W. Liu, P. Misra, E. Tanaka, J. P. Zimmer, B. Itty Ipe, M. G. Bawendi, J. V. Frangioni, *Nat Biotech* **2007**, *25*, 1165.
[11] E. M. Pridgen, R. Langer, O. C. Farokhzad, *Nanomedicine* **2007**, *2*, 669.
[12] a) H. Kobayashi, M. R. Longmire, M. Ogawa, P. L. Choyke, *Chem. Soc. Rev.* **2011**, *40*, 4626; b) H. Koo, M. S. Huh, I.-C. Sun, S. H. Yuk, K. Choi, K. Kim, I. C. Kwon, *Acc. Chem. Res.* **2011**, *44*, 1018.
[13] J. Yang, Y. Zhang, S. Gautam, L. Liu, J. Dey, W. Chen, R. P. Mason, C. A. Serrano, K. A. Schug, L. Tang, *Proc. Natl. Acad. Sci. USA* **2009**, *106*, 10086.
[14] Y. Zhang, R. T. Tran, I. S. Qattan, Y.-T. Tsai, L. Tang, C. Liu, J. Yang, *Biomaterials* **2013**, *34*, 4048.
[15] Y. Zhang, J. Yang, *J. Mater. Chem. B* **2013**, *1*, 132.
[16] K. Li, B. Liu, *J. Mater. Chem.* **2012**, *22*, 1257.
[17] H. Abe, N. Takahashi, K. J. Kim, M. Mochizuki, Y. Doi, *Biomacromolecules* **2004**, *5*, 1606.
[18] L. S. Nair, C. T. Laurencin, *Progress in Polymer Science* **2007**, *32*, 762.
[19] J. W. Leenslag, A. J. Pennings, R. R. M. Bos, F. R. Rozema, G. Boering, *Biomaterials* **1987**, *8*, 311.

[20] A. Remes, D. F. Williams, *Biomaterials* **1992**, *13*, 731.
[21] Z. Wang, S. Wang, Y. Marois, R. Guidoin, Z. Zhang, *Biomaterials* **2005**, *26*, 7387.
[22] Y. Lu, P. S. Low, *Adv. Drug Deliv. Rev.* **2002**, *54*, 675.
[23] a) J.-H. Park, G. von Maltzahn, L. Zhang, A. M. Derfus, D. Simberg, T. J. Harris, E. Ruoslahti, S. N. Bhatia, M. J. Sailor, *Small* **2009**, *5*, 694; b) N. Kohler, G. E. Fryxell, M. Zhang, *J. Am. Chem. Soc.* **2004**, *126*, 7206.

ADVANCED MATERIALS

Supporting Information

for *Adv. Mater.*, DOI: 10.1002/adma.201306070

Development of Intrinsically Photoluminescent and Photostable Polylactones

*Zhiwei Xie, Yi Zhang, Li Liu, Hong Weng, Ralph P. Mason, Liping Tang, Kytai T. Nguyen, Jer-Tsong Hsieh, and Jian Yang**

Submitted to ADVANCED MATERIALS

Supporting Information

for *Adv. Mater.*, DOI: 10.1002/adma.201306070

Development of Intrinsically Photoluminescent and Photostable Polylactones

Zhiwei Xie, Yi Zhang, Li Liu, Hong Weng, Ralph P. Mason, Liping Tang, Kytai T. Nguyen,

*Jer-Tsong Hsieh, Jian Yang**

Z. Xie, Prof. J. Yang
Department of Biomedical Engineering
Materials Research Institute
The Huck Institutes of The Life Sciences
The Pennsylvania State University
University Park, PA 16802

Y. Zhang, H. Weng, Prof. L.Tang, Prof. K.T. Nguyen
Department of Bioengineering
The University of Texas at Arlington
Arlington, TX 76019

L. Liu, Prof. R.P. Mason
Department of Radiology
The University of Texas Southwestern Medical Center
Dallas, TX 75390

Prof. J.T. Hsieh
Department of Urology
The University of Texas Southwestern Medical Center
Dallas, TX 75390

*Corresponding author: Jian Yang, W340 Millennium Science Complex, University Park, PA 16802. Tel.: (+1) 814-865-1278; E-mail: jxy30@psu.edu

Experimental Section

Synthesis of BPLPs and BPLP-polylactone copolymers (BPLPLs): BPLP prepolymers with terminal hydroxyl groups were synthesized by reacting citric acid with diol in a molar ratio of 1:1.1 as described previously.[1] L-Cysteine and L-serine were selected to synthesize BPLP-Cys and BPLP-Ser. Polyethylene glycol (MW=200 Da) was also used as a diol to prepare water-soluble BPLP (WBPLP). BPLPLs were synthesized via enzyme catalyzed ring-opening polymerization using pre-BPLP as macro-initiators. Typically, freeze-dried pre-BPLP was added into a dry 100 mL flask, and then lactones (for example, L-lactide) (purchased from Sigma-Aldrich, recrystallized twice in ethyl acetate before polymerization) were added into the flask with different ratios to BPLP. Next, porcine pancreas lipase (PPL, dried overnight under vacuum) was added into the flask with a ratio of 5% to lactone. The flask was vacuumed and purged with nitrogen three times, then sealed and heated to 100°C for 72 hrs. The copolymer was dissolved in chloroform and PPL was removed by filtration through a fritted filter. The polymer solution was concentrated under reduced pressure and then precipitated in cold ethanol. In case of using water-soluble pre-BPLP to synthesize amphiphilic copolymer, the product was dissolved by dimethyl sulfoxide (DMSO) and precipitate in cold DI water after filtration. Similar reactions were also conducted in 1, 4-dioxane at 100°C to synthesize BPLPLs in solutions. For the following in vitro and in vivo tests, polymers prepared by melt polymerization were used.

Preparation of films, nanoparticles, micelles and nanofibers: BPLP-PLLA films were prepared by casting their chloroform solution into Teflon molds and followed by evaporation. The BPLP-PLLA nanoparticles were prepared using the nanoprecipitation technique. 5 mg of the BPLP-PLLA polymer was dissolved in 5 mL of THF. The polymeric solution was added dropwise to 50 mL of deionized water. The solution was stirred at a speed of 700 rpm and the solvent was completely evaporated at room temperature. WBPLP-PLLA micelles were

fabricated through a similar method. Fluorescent nanofibers were fabricated by electrospinning 12% BPLP-Ser-PLLA50 chloroform solution at 18kV and 2.5 μL/min onto an aluminum board.

Polymer Characterization: Fourier Transform Infrared Spectra (FTIR) was collected at room temperature. The copolymer dissolved in chloroform was cast over a KBr pellet. The solvent was allowed to evaporate overnight in a chemical hood. FTIR spectra were collected using a Nicolet 6700 FTIR spectrometer (Thermo Fisher Scientific) at room temperature. For ^{1}H NMR measurements, 10 mg of copolymer was dissolved in 1 mL of deuterated chloroform or DMSO. The NMR spectra were collected on a JEOL 500 MHz spectrometer at room temperature.

Photoluminescent properties: UV-vis absorption spectra were collected using a Shimadzu UV-2450 spectrophotometer. A dilute solution of copolymer was prepared in DMSO. All photoluminescence spectra were obtained by Shimadzu RF-5301PC fluorospectrophotometer. Both the excitation and the emission slit width were set at 1.5 nm for all samples unless otherwise stated. Quantum yield of all samples was determined by Williams' method.[2] Anthracene (quantum yield = 27% in ethanol) was used as the standard. Photo-stability measurement was conducted by continuously illuminating the polymer solutions with excitation light at 365nm and emission at 430nm for 3 hours. Rhodamine B and Fluorescein aqueous solutions were tested for their photostability at their maximum excitation and emission wavelength for the same period of time.

Thermal properties: Thermal analysis was conducted on a differential scanning calorimeter (DSC, TA Instrument Q2000) at a heating ramp rate of 10˚C/min. A thermogravimetric analyzer (TGA, TA instrument Q500) was used to measure the thermal degradation of the polymers at a ramp rate of 10˚C/min from 0˚C to 500˚C.

In vitro degradation: The *in vitro* degradation of the polymers was done with 50 mg of copolymer placed in a tube containing 10ml of phosphate buffer saline (PBS) (pH=7.4). All samples were incubated at 37°C for predetermined times. At each time point, the samples were taken out, washed with water and lyophilized. The degradation was characterized by mass remaining. The *in vitro* degradation was also monitored by fluorescence loss.

Cell culture and in vitro studies: Polymer cytocompatibility was evaluated *in vitro* using NIH 3T3 fibroblast cells, which were cultured with Dulbecco's modified eagle's medium (DMEM) supplemented with 10% fetal bovine serum (FBS) and 1% antibiotics. The cells were suspended in media to obtain a seeding density of $5x10^5$ cell/mL. 200 µL of the suspension was added into 96 well plates. The cells were then incubated at 37 °C, 5% CO_2 and 95% humidity for 24 hours. Nanoparticles of BPLP-PLLA copolymers and controls (BPLP and PLLA) were added at various concentrations. MTT assay was used to assess the viability of the cells after 4hrs and 24hrs. The data obtained was normalized to the viability of cells cultured on tissue culture plate.

Cell uptake and fluorescence labeling: The cell uptake of the fluorescent nanoparticles was also examined *in vitro*. 3T3 fibroblasts were seeded onto sterile cover slips at a density of 5,000 cells/mL. Cells were allowed to attach and grow for 24 hours before uptake studies were performed. The cover slips were washed with PBS and transferred into a Petri dish. After 4 hours incubation with BPLP-Ser-PLLA50 nanoparticles (100 µg/mL), the medium was aspirated and the cells were washed three times with PBS to remove the excess nanoparticles, which had not been taken up. The cells were fixed with 2.5% glutaraldehyde for 2 hours. After fixing, the cover slips were mounted on glass slides and imaged under a Leica DMLP fluorescence microscope (Leica Microsystems, Bannockbum, IL) equipped with a Nikon E500 Camera (8.4V, 0.9A, Nikon Corp., Japan).

In vivo degradation: All animals were cared for in compliance with the regulations of the Animal Care and Use Committee of The University of Texas at Arlington. To measure the *in vivo* degradation, a disk of BPLP-Ser-PLLA20 (8 mm diameter and 1 mm thickness) was implanted subcutaneously in a 6-week-old nude mouse (32 nude mice were used in total). At each designated time point, the animals were imaged using a CRi Maestro ™ (Cambridge Research & Instrumentation, Inc, Woburn, MA) with an excitation filter of 503-555 nm and a longpass emission filter of 580nm.[3] The fluorescent intensity was calculated after subtracting auto-fluorescence sampled from the main body of the animal. At 2, 4, 6, 8, 10, 12, and 16 weeks post-implantation, four mice per time point were sacrificed to study the weight loss of BPLP-Ser-PLLA20 disks. All samples were carefully removed from surrounding tissue, washed by PBS, lyophilized and weighed.

In vivo biocompatibility evaluation: For evaluation of the in vivo host response, BPLP-PLLA disks (0.5 mm thickness and 8 mm diameter) were placed subcutaneously in 6-month-old female Sprague Dawley rats (Harlan Sprague Dawley, Inc., Indianapolis, IN) under deep isoflurane-O2 general anesthesia. All animals were treated and used according to the protocol approved by the University of Texas at Arlington and the University of Texas Southwestern Medical Center Animal Care and Use Committee (IACUC). Animals were observed daily for any change in their behavior over the period of experiment. At each pre-determined time point (1 and 10 weeks), four animals were sacrificed with excess CO2, and polymers with surrounding tissues were harvested for further evaluation. The explants were fixed by soaking in 10% formalin for 2 days, then embedded in paraffin wax, and sectioned into 4 μm sections. Six slides from different areas of the explants were stained with hematoxylin & eosin (H&E) and CD11b immunohistochemistry. The cross-sections were examined using a Leica DMLP microscope (Leica Microsystems Inc., Bannockburn, IL) fitted with a Nikon E500 camera (Nikon Corp., Japan).

Tumor targeted imaging: An MCF7 human breast tumor xenograft ($1x10^5$ MCF7 cells were injected on the back of a 6 week nude mouse) was used for in *vivo* tumor targeting and imaging. BPLP-Ser-PLLA50 nanoparticles were conjugated with folate by EDC/NHS chemistry before injected intravenous injection in the tail vein into mice at a concentration of 5 mg/mL and volume of 200 μL. After 4 and 6 hours, the animals were imaged using a Maestro ™ *in vivo* fluorescent imaging system, as described above. The animals were also sacrificed 8 hours post-injection and some organs including heart, liver, lung, spleen, kidney and tumor tissues were taken out to study the nanoparticle biodistribution via fluorescent imaging.

Table S1. Molecular and fluorescent characterization of different BPLP-PLLA copolymers.

Sample ID	BPLP to Lactide feeding ratio	Citric Acid to Lactic Acid ratio *	Mw from NMR (Da) #	Mw From GPC (Da) †	Yield (%)	Quantum Yield (%)
BPLP-Cys-PLLA20	1/20	1/8.76	3823	5319	48	39.9
BPLP-Cys-PLLA50	1/50	1/22.05	7650	10274	46	51.4
BPLP-Cys-PLLA100	1/100	1/31.21	10288	12369	33	13.5
BPLP-Ser-PLLA20	1/20	1/8.77	3826	5971	77	9.3
BPLP-Ser-PLLA50	1/50	1/19.04	6784	7894	43	4.9
BPLP-Ser-PLLA100	1/100	1/32.73	10726	14257	38	1.5
WBPLP-Cys-PLLA20	1/20	1/5.34	2838	N/A	39	27.4
WBPLP-Cys-PLLA50	1/50	1/7.38	3425	N/A	27	21.1
WBPLP-Cys-PLLA100	1/100	1/9.09	3918	N/A	35	15.4

* Determined by ^{1}H NMR.

Estimated from NMR data. The Mw of BPLP macro-initiator was 1300 Da (determined by MALDI-MS).

† BPLP-Cys-PLLA and BPLP-Ser-PLLA were tested in chloroform by using a Shimadzu HPLC system equipped with a Phenomenex Phenogel 5µ 10E3 SEC column, and a Wyatt miniDAWN lighter scattering detector and an OptiLab RI detector. Mw of WBPLP-Cys-PLLA was not determined by GPC.

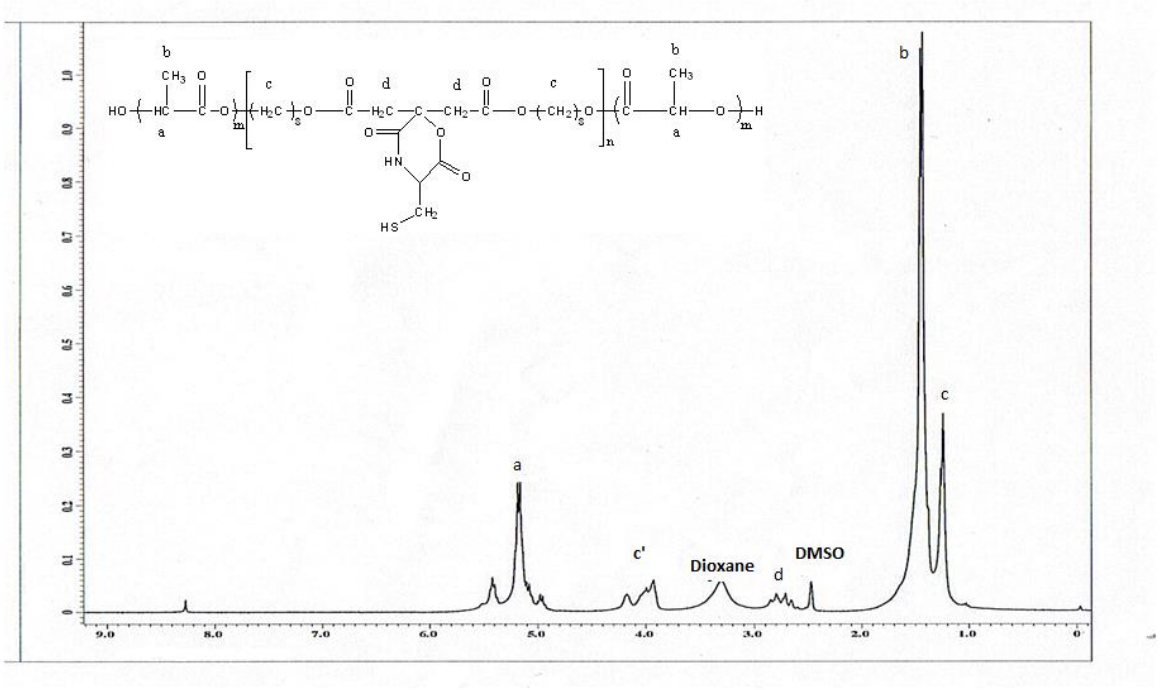

Figure S1. ^{1}H NMR spectrum of a representative BPLP-PLLA copolymer, BPLP-Cys-PLLA100. Both peaks of BPLP and PLA are present, including the peaks at 1.02 ppm (-CH_2SH from L-cysteine), 1.23 ppm, 1.40 ppm, and 4.05 ppm (-CH_2- from 1, 8-octanediol), 2.76 ppm (-CH- from citric acid), 1.45 ppm (-CH_3 from PLA block), 5.2 ppm (-CH- from PLA block)

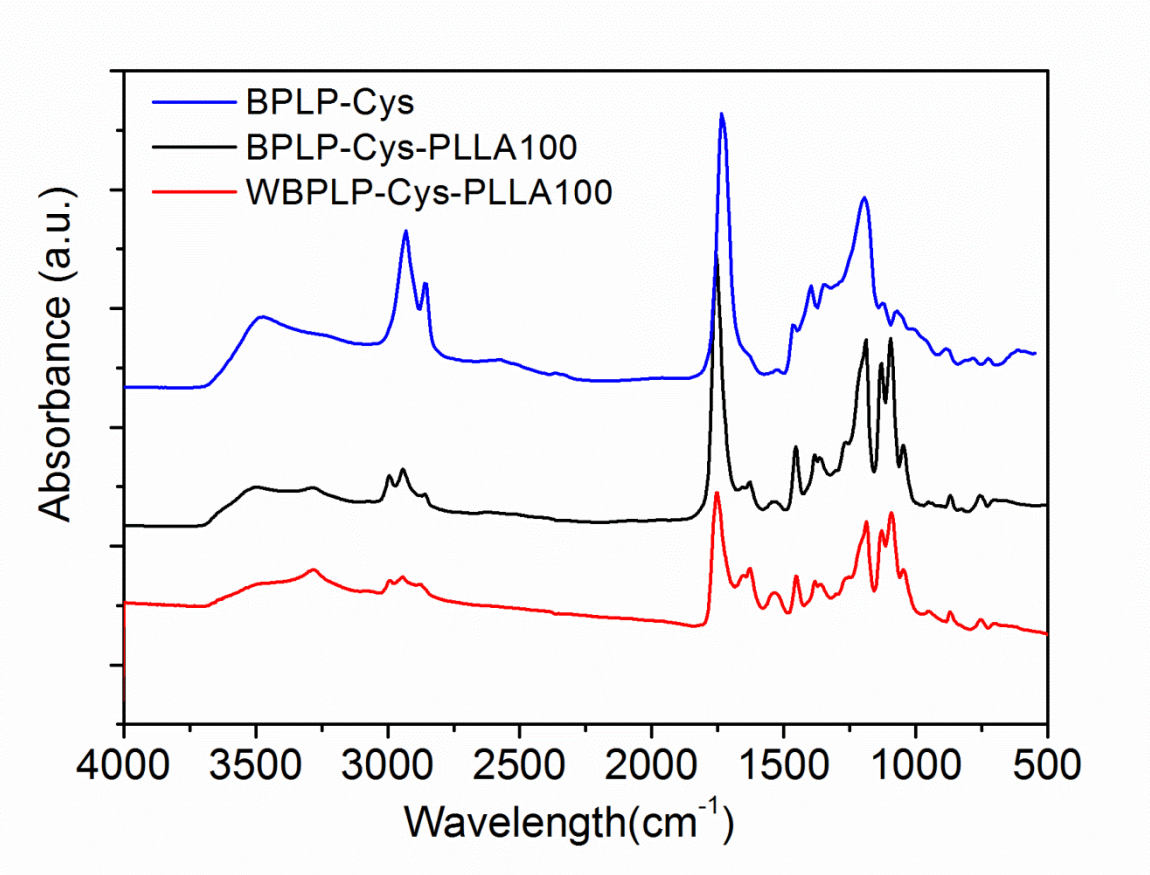

Figure S2. ATR-FTIR spectra of BPLP-Cys, BPLP-Cys-LA100 and WBPLP-Cys-LA100. The peaks at 2575 cm^{-1} (-SH), 1527 cm^{-1} (-C(=O)NH-), 2931 cm^{-1} ($-CH_2-$), 3467 cm^{-1} (-OH) are from BPLP-Cys. Also, the -C=O shifted from 1735 to 1756 cm^{-1}, indicating esterification of carboxyl groups are from PLA blocks after copolymerization.

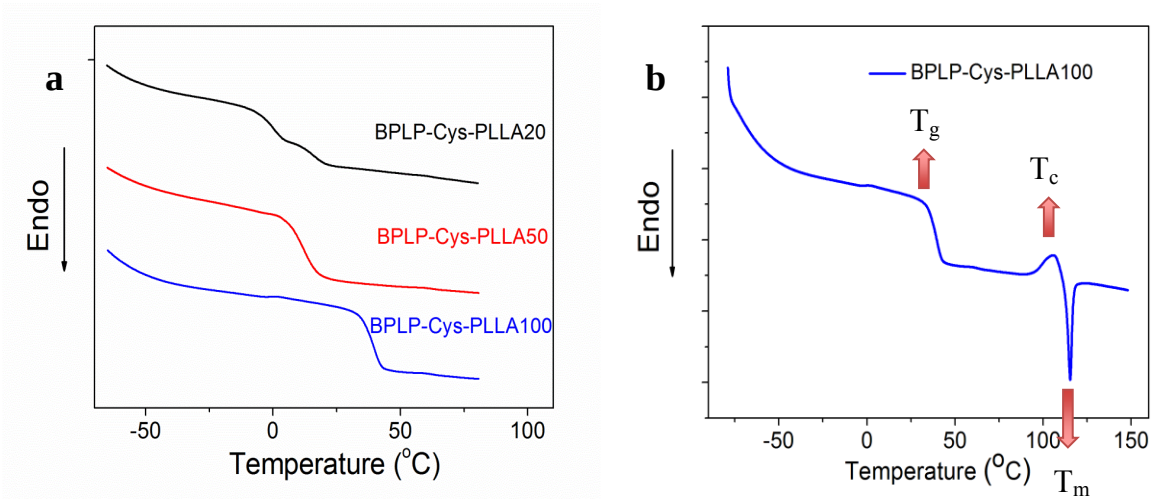

Figure S3. (a) Differential scanning calorimetry (DSC) spectra of BPLP-Cys-PLLA with various polylactide chain lengths. (b) A representative DSC thermogram of BPLP-Cys-PLLA100. Tg, Tc and Tm indicate the glass transition temperature, crystallization temperature and melting temperature respectively.

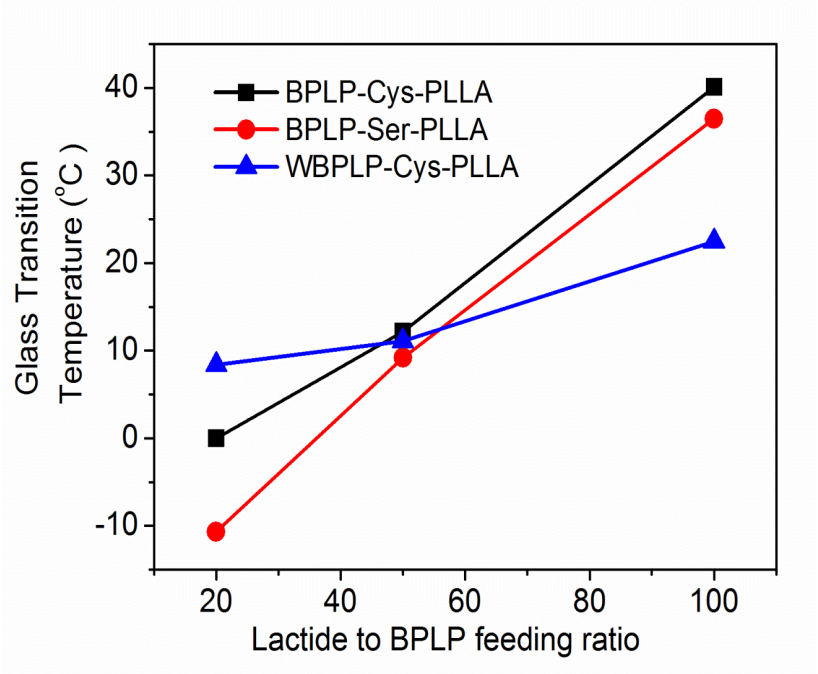

Figure S4. Glass transition temperatures of various BPLP-PLLA copolymers with different lactide to BPLP feeding ratios.

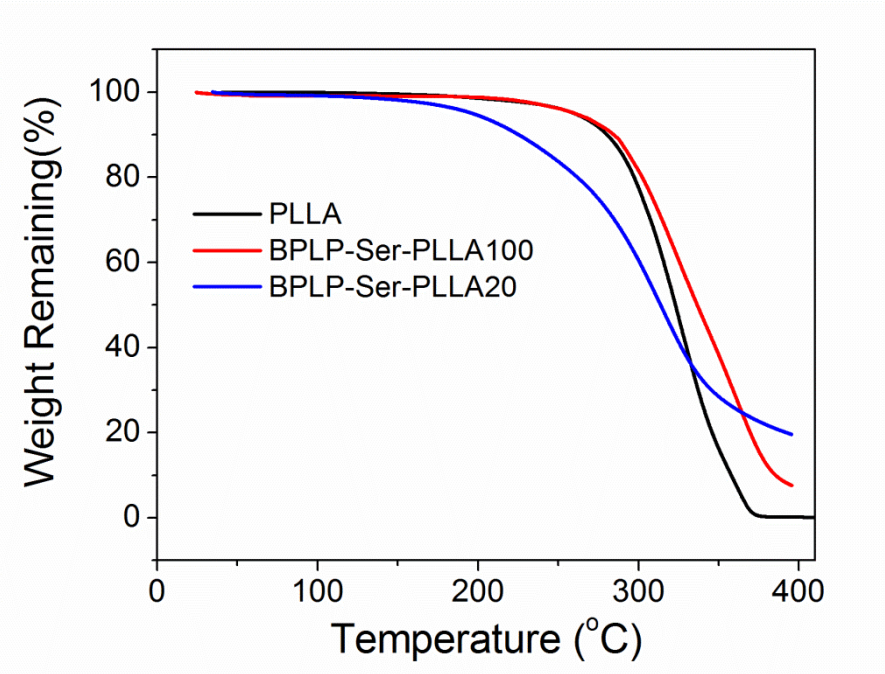

Figure S5. Thermal gravity analysis of BPLP-Ser-PLLA20, BPLP-Ser-PLLA100, and PLLA.

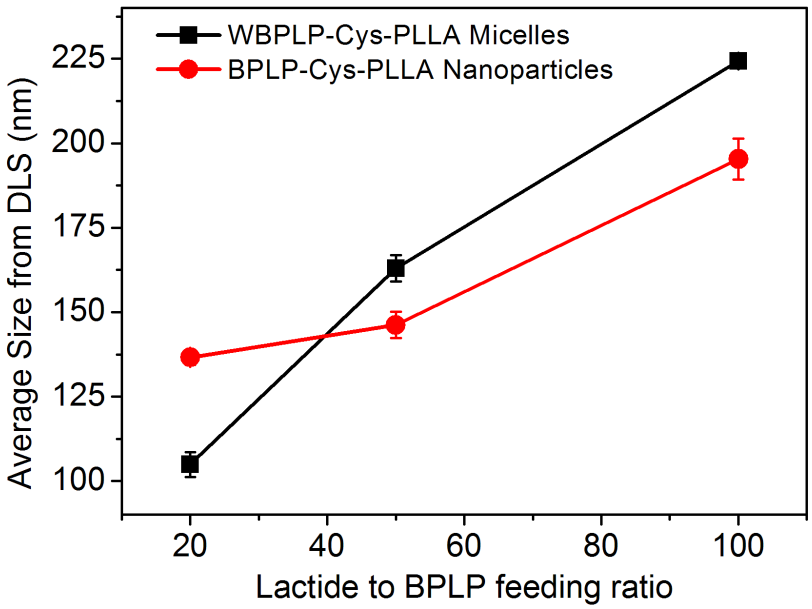

Figure S6: The sizes of BPLP-Cys-PLLA nanoparticles and WBPLP-Cys-PLLA micelles with different lactide to BPLP feeding molar ratios.

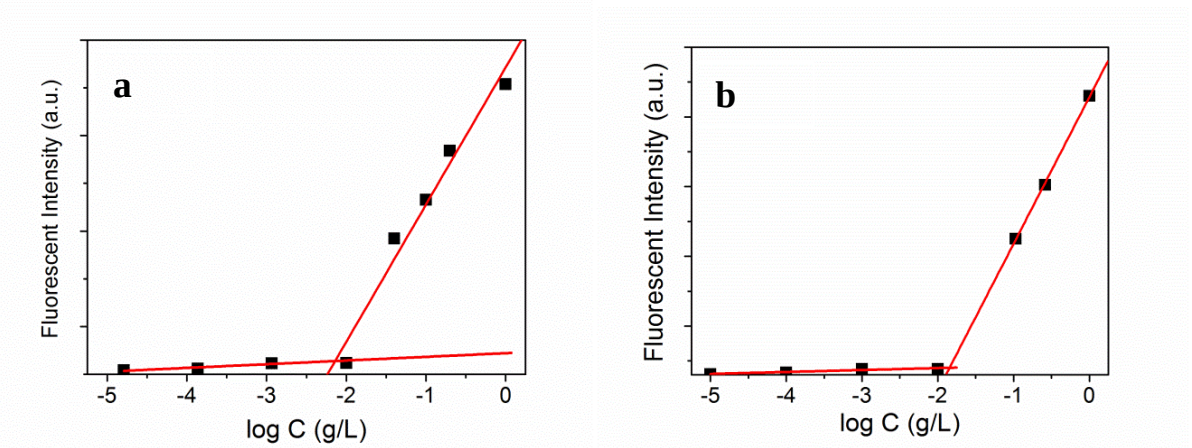

Figure S7. Determination of critical micellar concentration (CMC) of WBPLP-Cys-PLLA20 (a) and WBPLP-Cys-PLLA50 (b). Fluorescent intensities of Nile Red in solution were plotted as a function of their concentration. The CMC for WBPLP-Cys-PLLA20 and WBPLP-Cys-PLLA50 are 1.283×10^{-2} g/L and 7.262×10^{-3} g/L respectively.

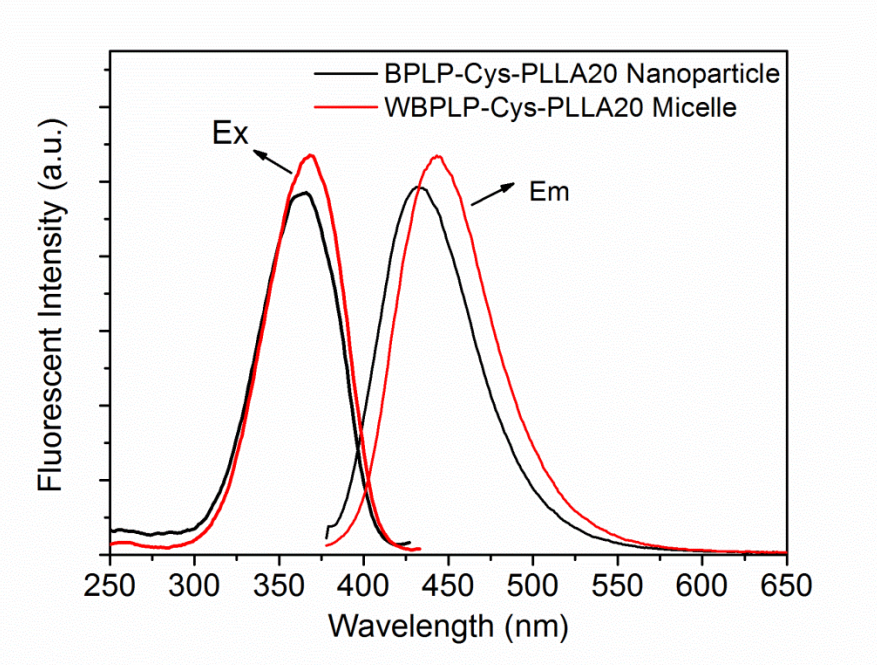

Figure S8. Fluorescent emission and excitation spectra of (A) BPLP-Cys-PLLA20 nanoparticles and (B) WBPLP-Cys-PLLA20 micelles.

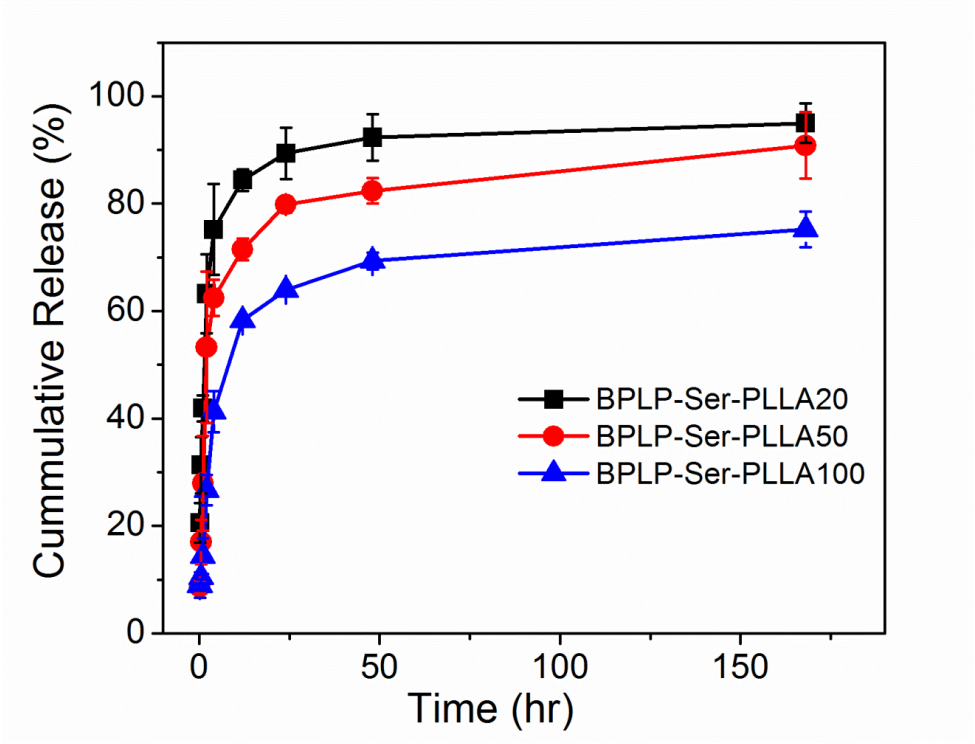

Figure S9. 5-Fluorouracil drug release curves from BPLP-Ser-PLLA nanoparticles with different molecular weights. Nanoparticles were incubated in pH 7.4 50mM PBS solutions.

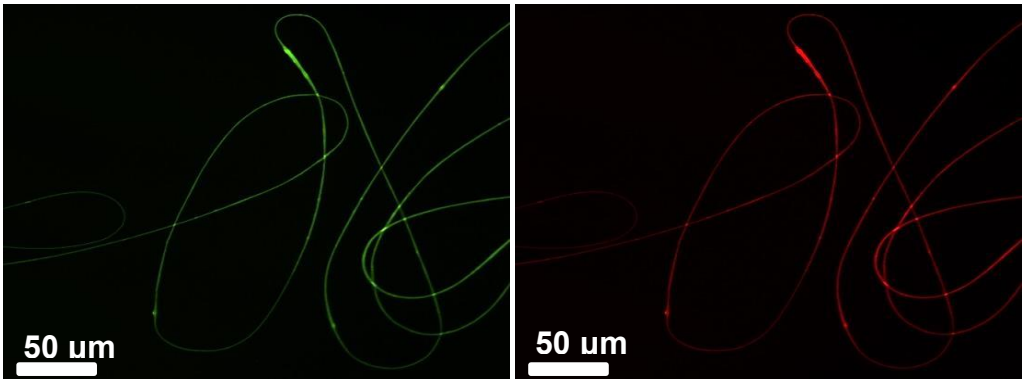

Figure S10. Microscopic fluorescence images of electrospun BPLP-Ser-PLLA50 fibers with FITC and Cy3 filters from left to right respectively. These ultra-fine fibers potentially can be used to fabricate in vivo trackable tissue engineering scaffolds and drug delivery devices.

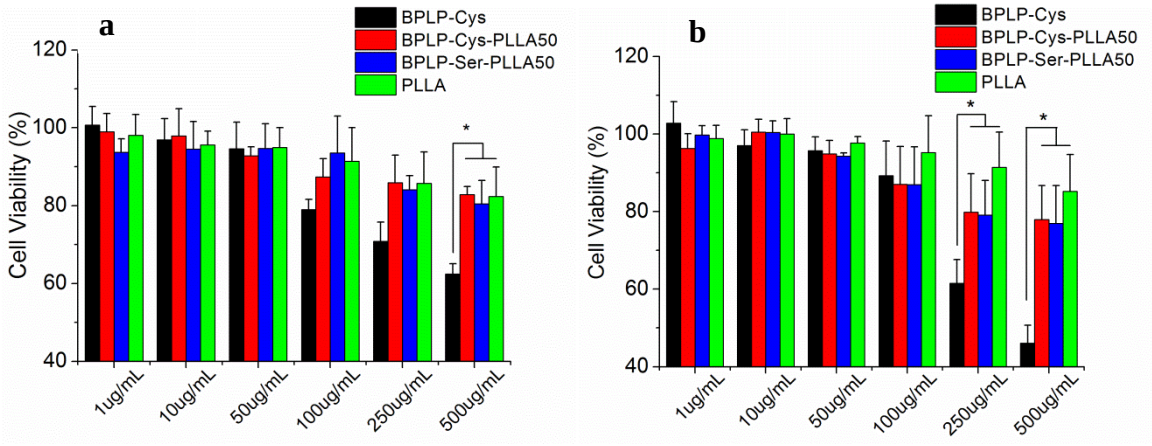

Figure S11. Viability of mouse 3T3 fibroblasts incubated with BPLP-Cys, BPLP-Cys-PLLA50, BPLP-Ser-PLLA50 and PLLA nanoparticles at different concentrations for (**a**) 4 hrs, (**b**) 24 hrs (*, p<0.01). The lower viability of BPLP-Cys at high concentrations is probably due to the free carboxyl groups of BPLPs which lower the pH of the culture medium.

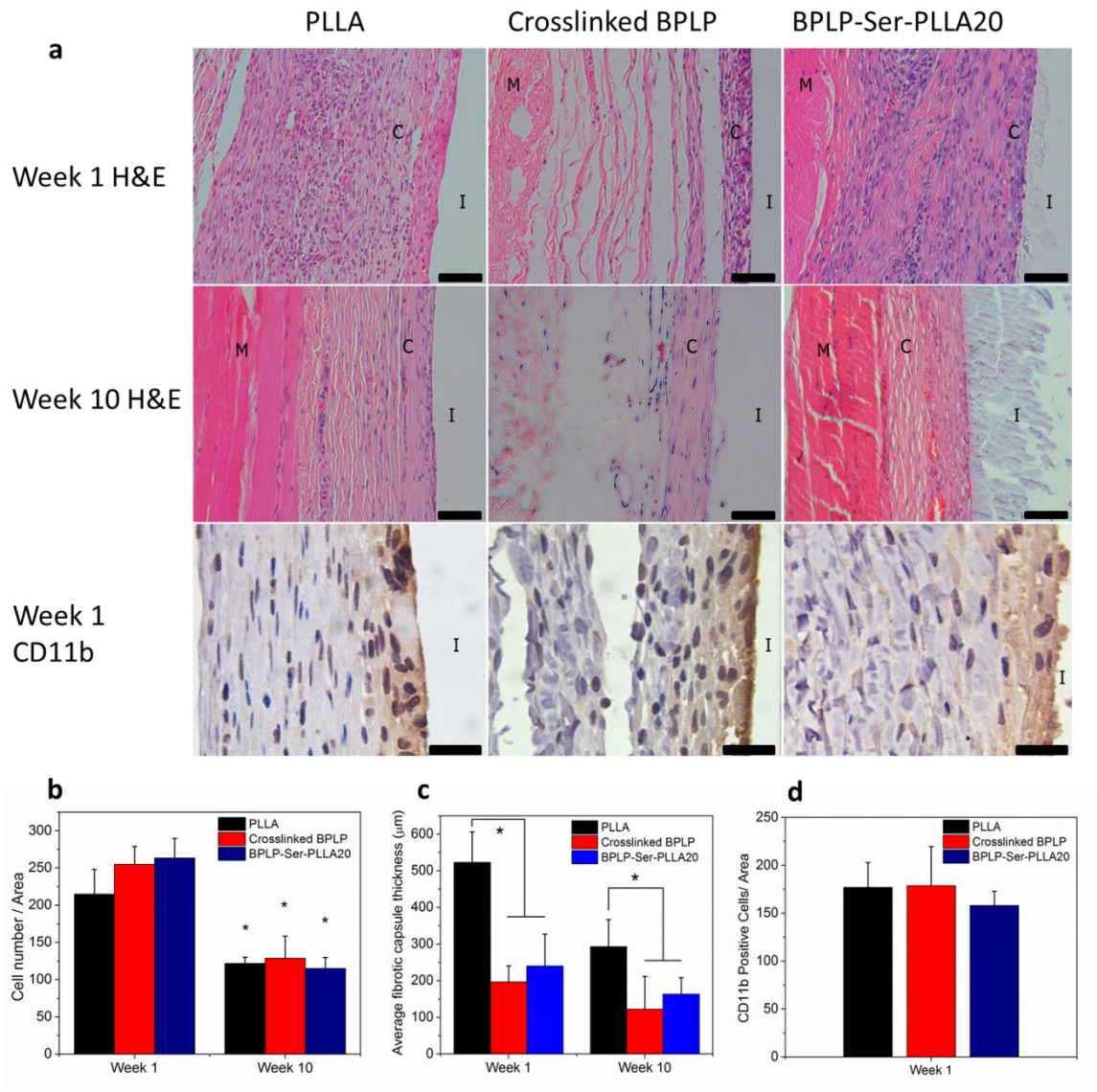

Figure S12. *In vivo* biocompatibility evaluation of subcutaneously implanted BPLP-PLLAs. **a**) Representative H&E (scale bar = 100 μm) and anti-CD11b (scale bar = 25 μm) staining images of implanted PLLA, crosslinked BPLP-Ser, and BPLP-Ser-PLLA20 films (I: implant, C: fibrous capsule, M: muscle). **b**) Total cell numbers in an area of 200μm x 200μm from the edge of the implants (*, p<0.01). **c**) Average of fibrotic capsule thickness of the implants (*, p<0.01). **d**) Number of CD11+ inflammatory cells surrounding the implants.

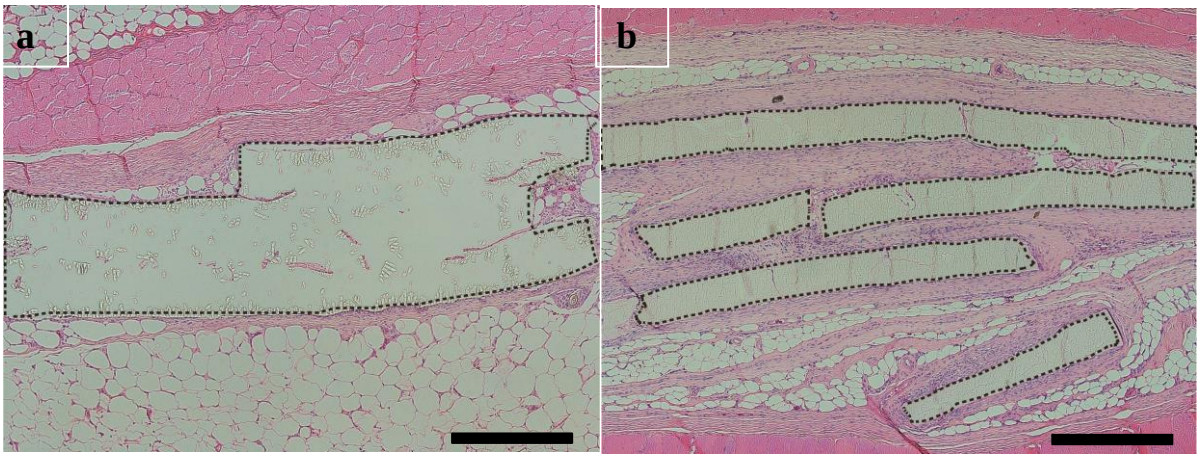

Figure S13. H&E staining images of subcutaneously implanted BPLP-Ser-PLLA20 film at (a) 1week and (b) 10 weeks. Scale bar = 500 μm. Polymer pieces are highlighted by dash lines.

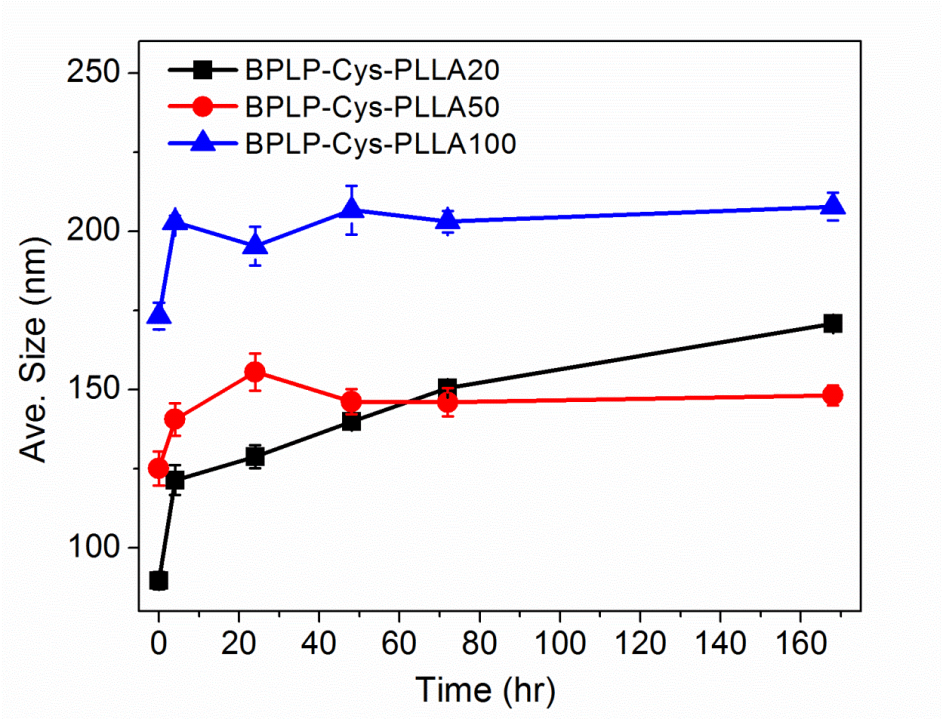

Figure S14. Evaluation of hydrodynamic stability of BPLP-Cys-PLLA nanoparticles in pH 7.4 50mM PBS solutions by measuring the size changes of nanoparticles over time.

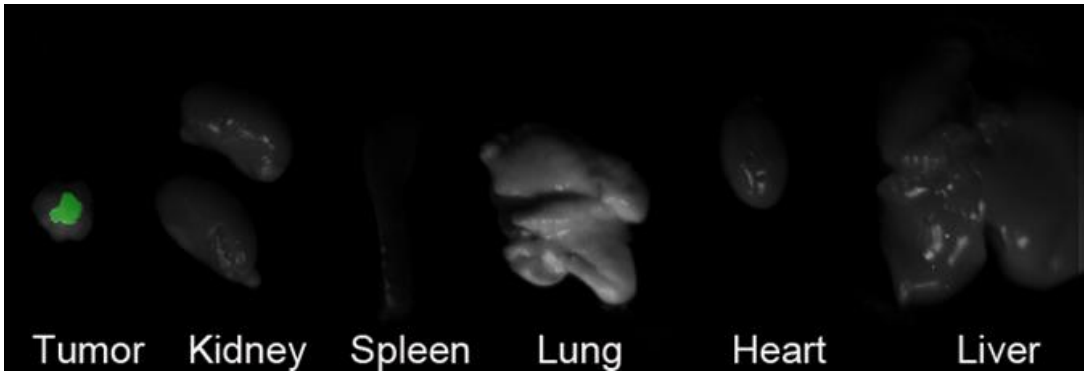

Figure S15. Merged *ex vivo* fluorescent and white light images of tumor and organs from a nude mouse with a human MCF7 breast tumor xenograft growing on its back after tail i.v. injection of BPLP-Ser-PLLA50 nanoparticles.

[1] J. Yang, Y. Zhang, S. Gautam, L. Liu, J. Dey, W. Chen, R.P. Mason, C.A. Serrano, K.A. Schug, L. Tang, *Proc. Natl. Acad. Sci. USA* **2009**, 106, 10086.

[2] A. T. R. Williams, S. A. Winfield, J. N. Miller, *Analyst* **1983**, 108, 1067.

[3] J. Zhang, J. Su, L. Liu, Y. Huang, R. P. Mason, *J. Nanosci. Nanotechnol.* **2008**, 8, 1155.